THE EFFECT OF ALLOY COMPOSITION ON THE PERFORMANCE OF STAINLESS STEELS IN EXHAUST GAS ENVIRONMENTS

B. A. Pint, R. Peraldi and P. F. Tortorelli
Oak Ridge National Laboratory
Oak Ridge, TN 37831-6156

ABSTRACT

Recuperators for developmental high-efficiency small gas turbine engines will require low-cost materials with both creep and corrosion resistance at 700°C or higher. Because of the accelerated corrosion attack caused by water vapor in the exhaust gas and pressurized inlet air, alloys used in current recuperators, such as type 347 stainless steel, do not have sufficient oxidation resistance to meet lifetime goals at these higher temperatures. More highly alloyed steels and Ni-base alloys can meet the requirements but may be prohibitively expensive. Model Fe-Ni-Cr and Fe-Cr alloys are being tested in air plus 10% water vapor in order to determine compositions with appropriate environmental resistance for this application and to determine the effect of minor alloy additions. Results indicate that Ni and Cr contents in the 20 wt.% range prevent accelerated attack observed in leaner alloys and that Si is the most critical minor (<0.5 wt.%) alloy addition for long-term oxidation resistance in these environments.

Keywords: Stainless steel, gas turbines, recuperators, water vapor, alloy composition

INTRODUCTION

Small (30-200kW) gas turbine engines or microturbines are one solution to the issues of improving power quality and overloaded transmission lines.[1-2] Sited at or near the user's facility, a microturbine could provide base load or peak load power with much lower emissions than similar-sized diesel or natural gas fired reciprocating engines. The waste heat from the microturbine also could be used for climate control or heating water at the facility. However, compared to large gas turbine engines, microturbines have relatively low operating efficiencies and relatively high initial and installation costs (per kilowatt). As part of the Department of Energy's Distributed Energy Resources program, the Advanced Microturbine Systems program is seeking to improve the efficiency of microturbines and to lower their costs by developing partnerships among engine manufacturers, materials suppliers and materials scientists.[3]

One well-known way to improve the efficiency of microturbines from 15-20% to 25-30% is by incorporating a recuperator or heat exchanger to use the exhaust gas to heat the compressed air entering the combustor.[4] Most recuperators have used stainless steels, such as type 347, because of its excellent combination of creep and corrosion resistance. In order to further increase efficiency, higher turbine inlet temperatures are needed which also may require recuperators to operate at higher temperatures. A temperature increase is a particularly critical problem for most recuperators because they tend to employ thin-walled components to maximize the heat transfer in a minimal volume and weight. With a 75-125μm thick type 347 foil used in both primary surface and plate-and-fin type recuperators,[5] there is only a limited reservoir of Cr available to achieve desired operating lifetimes of 20,000-50,000h. Also with the limited Cr reservoir, any accelerated corrosion attack will result in a greatly reduced component lifetime. With recuperator operating temperatures moving towards 700°C and higher, Fe-base chromia-forming alloys like type 347 stainless steel can be susceptible to accelerated attack (i.e. high rates of metal wastage) due to water vapor.[6-16] The common observation is the breakdown of the normally protective Cr-rich surface oxide and the formation of Fe-rich oxides. Water vapor is present in the exhaust gas as a combustion product but also can have a significant concentration in the compressed inlet air because of the higher total pressure.

The effect of water vapor on the oxidation behavior of ferritic and austenitic alloys is being widely studied and, while the exact mechanism may not be understood, it is clear that increasing the alloy Cr content should increase resistance to accelerated attack.[11,13-16] However, for recuperator applications, alloys with increased Cr levels represent both a cost increase and a potential reduction in mechanical properties as well as formation of detrimental Cr-rich intermetallics, such as σ phase.[17] Therefore, the goal of the current research program is to examine the effects of alloy composition on performance in water-laden environments in order to specify a low-cost alternative to type 347 stainless steel. The present work has been conducted on model alloys in order to (1) identify the base Cr and Ni contents required to resist accelerated attack and (2) identify minor alloying additions that may be beneficial for this application and temperature range.

EXPERIMENTAL PROCEDURE

The chemical compositions of selected alloys are listed in Table I in order to indicate typical impurity levels. Some of the alloys were obtained from commercial vendors and then hot and cold rolled at Oak Ridge National Laboratory (ORNL) to ≈100μm thickness with a grain size of ≈10μm. The model alloys were vacuum induction melted at ORNL and hot and cold rolled to 1.25mm sheet. After the final cold rolling step, the sheets were annealed in Ar for 2min at 1000°C for the austenitic alloys and 2min at 900°C for the ferritic alloys. Example alloy grain structures are shown in Figure 1 and the average grain sizes of the rolled model alloys are given in Table I. Foil specimens (≈12mm x 18mm) were tested in the as-rolled conditions and similar-sized sheet specimens were polished to a 600 SiC grit finish. The specimens were cleaned in acetone and methanol prior to oxidation and mass changes were measured using a Mettler-Toledo model AG245 balance after each 100h cycle at 650°, 700° or 800°C.

Oxidation exposures in air (with and without injected water) were conducted by flowing the gas at 450 cc/min through an alumina tube that was inside a resistively-heated horizontal tube furnace. Distilled water was atomized into the flowing gas stream above its condensation temperature and heated to the reaction temperature within the alumina tube. Water was collected and measured after flowing through the tube to calculate its concentration and calibrate the amount of injected water. A water content of 10 vol.% was used for these experiments. Up to 40 specimens were positioned in alumina boats in the furnace hot zone so as to expose the specimen faces to the flowing gas. After oxidation, selected specimens were Cu-plated and sectioned for metallographic analysis.

RESULTS

Foil specimens of commercial alloys

To illustrate the effect of water vapor on the performance of stainless steel foils, results for foils of type 321 and 347 stainless steels are shown in Figure 2. Compared to oxidation in dry air at 800°C, the mass gains in humid air (10% H_2O) at 700° and 800°C are significantly higher. The rate of mass gain in water vapor dropped after a few cycles at 800°C only because a large fraction of the metal had already been consumed. Light microscopy of polished cross-sections of several foils are shown in Figure 3. After 5,000h at 800°C in dry air, a thick but dense and adherent scale formed on type 321 stainless steel, Figure 3a. After only 1000h in humid air, more than 50% of the type 347 foil had been consumed, Figure 3b. A similar degree of attack was observed for type 321 foil. At lower temperatures, Figures 3c and 3d, the amount of metal consumed was reduced but the thick oxide after only 1000 h indicates that type 347 foil is unlikely to meet long-term life targets needed for a microturbine recuperator.

Based on previous testing on foils,[11,15,18] it is clear that higher alloyed stainless steels and Ni-base alloys are more resistant to this environment than type 347 stainless steel. Figure 4 shows the relatively thin scales formed on several commercial alloys after long-term exposures at 800°C in humid air. A 20/25/Nb foil did not show accelerated attack, Figure 4a, but after 6,000h at 800°C some nodules had begun to form. The Ni-base alloys 625 and 214 showed no indication of any accelerated attack during testing at 800°C, Figures 4c and 4d. The Al_2O_3-forming alloy 214 shows a very thin surface oxide after 5,000h at 800°C. Higher temperatures (>800°C) require alumina-formers in order to achieve acceptable rates of corrosion loss in this application.[15,18] However, these Ni-base alloys are all more expensive than type 347,[15] and in order for microturbines to meet their initial cost targets, a lower-cost alloy is desired.

Sheet specimens of model austenitic alloys

In order to explore the effect of alloy composition, model austenitic and ferritic alloys were tested under similar conditions. In this case, the specimens were cut from 1-1.25 mm thick sheet rather than foil. Sheet specimens show similar behavior in these experiments as foils. Figure 4d shows a 1mm thick sheet of alloy 625 with an oxide of similar thickness to that on the foil material formed after 6,000h at 800°C in humid air, Figure 4b. The internal oxides have a slightly finer structure on the foil material because of its finer grain size. However, the rolled model austenitic alloys in sheet form had 10-20µm average grain sizes (Table I and Figure 1b) that are similar to those found in foils.[5] Therefore, the model alloys were not rolled to foil.

Model alloys with various Cr (16-20%)and Ni (10-30%) contents were examined in both as-cast and rolled forms at 650°-800°C.[16] Figure 5 shows the type of data obtained from these studies for rolled alloys in humid air at 800°C. The accelerated attack caused by water vapor resulted in high mass gains when the scale was adherent or mass losses when the thick oxide spalled. By increasing either the Cr or Ni contents, the amount of accelerated attack was reduced. Similar results were obtained at 700°C and are shown schematically in Figure 6. Over the range of Cr and Ni contents examined, a line can be drawn separating the alloys that undergo accelerated attack (AA) and those that form a protective oxide scale (POS). For the rolled alloys with a fine grain size, lower Cr and Ni contents are required to form a POS than for the coarser-grained, as-cast alloys.[16] The finer alloy grain structure allows faster short-circuit diffusion in these alloys[19] which presumably prevents Cr depletion at the metal-scale interface. Diffusion of Cr in the substrate appears to be especially important at the lower temperatures, 650°-700°C. For both rolled and cast materials, protective behavior was observed with lower Cr contents when the Ni content was increased, indicating a synergistic benefit of higher Ni contents.

The mass gains shown in Figure 5 are complicated by scale spallation. Not surprisingly, the alloy that formed the thinnest scale after 500h at 800°C, Fe-20Cr-30Ni, also contained the highest Cr and Ni contents, Figure 7a. The scales formed on the other alloys were 5-10X thicker. Large mass losses were observed for Fe-20Cr-10Ni, Figure 5, but the remaining scale was very thick, Figure 7c. A similar scale thickness was observed on Fe-16Cr-30Ni, Figure 7e, indicating the beneficial effect of higher Ni contents when the Cr content was reduced. With the lowest Cr and Ni contents, Fe-16Cr-10Ni also showed the thickest oxide, Figure 7f. Using X-ray diffraction and electron probe microanalysis,[16] the thicker oxides generally were found to contain three layers from the gas interface to the metal interface: Fe_2O_3, $(Fe,Cr,Ni)_{0.8\text{-}1}O$ and $(Fe,Cr,Ni)_{1.4\text{-}1.7}O_x$. The composition of the middle layer suggests a mixture of (Fe,Cr,Ni)O and $(Fe,Cr,Ni)_3O_4$, while the inner layer may be a mixture of Fe metal and oxide.[20] An example of the relative compositions of the 2 inner layers for the Fe-20Cr-10Ni specimen are 40-50at%Fe, 30-40%Cr and 20%Ni.

Sheet specimens of model ferritic alloys

Another goal of this work was to isolate the effects of minor element additions. In order to simplify the study, a base ferritic composition of Fe-16Cr was chosen. The additions had little or no effect on the alloy grain sizes, Table 1. Manganese is commonly found in stainless steels but several different Mn contents were examined as this element has been reported to reduce scale evaporation in ferritic alloys developed for fuel cells.[21] Figure 8 shows a summary of mass gain results at 700° and 800°C in humid and dry air. These mass gain results are easier to interpret as none of the ferritic alloys showed scale spallation during the 5, 100h cycles. For reference, the performance of three binary Fe-Cr alloys has been included. As expected, the mass gain dropped when the Cr content was increased from 10% to 20%. However, at 700°C, the binary alloys were still heavily attacked by the addition of water vapor, Figure 8a. The various additions showed little benefit at this temperature except for the alloy containing Si. Silicon previously has been shown to have a strong beneficial effect on the corrosion resistance of ferritic alloys under similar conditions.[14,22] Silicon as well as Mo showed a beneficial effect at 800°C, Figure 8b. The 2%Mo addition (similar to type 444 stainless steel) reduced the alloy grain size compared to the other alloys (Table 1) which may be the principal reason for its beneficial effect. At this temperature, the ferritic alloys generally showed better corrosion resistance than at 700°C. The lower mass gains at 800°C are not due to increased scale evaporation at the higher temperature. With the relatively low gas flow rate used in this test, mass losses due to evaporation are estimated to be $<0.1\,mg/cm^2$ after 500h.

Figure 9 shows an example of the mass gains obtained at 700°C. For many of the alloys, a large mass gain was observed during the first 100h followed by little mass change and no observed scale spallation. One explanation for this type of behavior is that the surface of the rolled specimens contained some defects and that once the outer layer of metal was consumed, the mass gain was greatly reduced. In order to test this hypothesis, the scale after a 100h exposure was removed from three specimens and they were subsequently reexposed in the same test. For Fe-16Cr-1Mn, the initial scale that was removed is shown at 0h. However, during the next cycle, a thick oxide reformed, Figure 9. For Fe-16Cr+La, a thin scale initially formed and reformed after repolishing but, during subsequent cycles, a thicker oxide reformed. For Fe-16Cr+Si, low mass gains were observed with and without the repolishing step.

The beneficial effects of minor elements are currently being examined in a second series of model alloys focusing on 16-20Cr and 15-20Ni. An initial result is shown in Figure 5, where a Fe-20Cr-20Ni with Mn and Si additions, shows lower mass gains than any of the ternary Fe-Cr-Ni alloys. A SiO_2 sublayer has been observed in many studies,[14,18,22,23] and may prevent or delay the onset of accelerated attack.

DISCUSSION

The current results suggest that it may be possible to develop a stainless steel to meet the microturbine recuperator temperature and lifetime goals with a only a modest cost increase compared to type 347 foil. The model alloy testing suggests that increasing the Ni content (above the 10-12% in type 347) as well as the Cr content will increase the resistance to accelerated attack in environments with water vapor. The results for the model alloys containing minor alloying elements suggest that Si is the most beneficial minor element in these conditions. However, the addition of Si can lead to the formation of detrimental intermetallic phases in the steel,[17] so the amount of Si needs to be carefully considered. Even small quantities of Si likely leads to the formation of an inner SiO_2 layer[23] which may prevent or delay the onset of accelerated attack in exhaust gas environments. However, Si is already present in commercial stainless steels so that its addition is unlikely to make an unprotective alloy like 347 significantly better but it may have a slight effect on the location of the critical composition lines in Figure 6. It also is important to note that the mass gains for the model alloys are somewhat higher than expected because they have little or no detectable Si, Table I.

Predicting the long-term performance of stainless steels under these conditions is difficult. The lifetime goals (≥20,000h) require some data extrapolation. However, several studies have noted an incubation period prior to the onset of accelerated attack.[11,24,25] Thus, short-term tests prior to the onset of accelerated attack may be very deceptive in predicting the long-term performance of stainless steels in humid air. Exposures of 347 foil for 1000h at 650°C in humid air do not always produce accelerated attack. If the very low mass gains from a short-term test are used to predict foil lifetime, the alloy may appear to have acceptable corrosion resistance.

A common strategy in corrosion testing is to increase the test temperature to simulate longer exposure times at lower temperatures. However, the effect of water vapor is very temperature sensitive and higher temperature testing may lead to incorrect conclusions. For example, the testing of the model ferritic alloys showed more protective behavior in humid air at 800°C compared to 700°C. There are at least three relevant competing processes that increase with temperature: (1) external scale formation, (2) diffusion of Cr in the alloy, and (3) formation of volatile $CrO_2(OH)_2$. At lower temperatures (650°-700°C), a thinner scale and slower Cr diffusion in the relatively coarse-grained ferritic model alloys can result in loss of the scale (or Cr depletion of the scale) due to evaporation and Cr depletion in the alloy at the surface. These two factors would likely contribute to the onset of accelerated attack. If the scale growth rate and Cr diffusion increase with temperature more rapidly than the evaporation rate, then at higher temperatures (800°C), the ferritic alloy may be less susceptible to accelerated attack. A second example of the temperature effect is the behavior of the model austenitic alloys at 800°C, Figure 5. For the Fe-20Cr-30Ni alloy, there is only a factor of two difference between the scale formed in humid and dry air, Figure 7a and 7b. For this alloy at 800°C, water vapor appears to increase the chromia scale growth rate but not cause accelerated attack (i.e iron oxide formation) as at lower temperatures.[16] These two observations were made on rolled (fine-grained) and cast (coarse-grained) materials; however, the alloy grain size was not an important variable at 800°C for Fe-20Cr-30Ni. Figure 7g shows a similar scale thickness formed on cast Fe-20Cr-30Ni after the same 500h exposure in humid air. In contrast, alloy grain size was a more critical factor at 650° and 700°C where Cr diffusion/depletion in the alloy may be more important in determining the onset of accelerated attack.[16] The importance of alloy grain size at low temperatures also may explain the poor performance of the ferritic alloys at 700°C because of their relatively large grain size, Figure 1. A similar observation on the relative scale thicknesses formed in humid and dry air was made for Fe-20Cr-10Ni, Figures 7c and 7d. Thus, as 800°C is not a representative temperature for the corrosion observed at lower temperatures, the second phase of model

alloy testing will focus on 650° and 700°C performance.

One opportunity for accelerated laboratory testing may be the amount of water vapor or the gas flow rate. It could be argued that 10% water vapor is higher than expected in an exhaust gas stream. However, 10% is both a uniform standard exposure and an attempt to accelerate the onset of accelerated attack. Experimental work has shown that the incubation period decreased with increasing water content.[11,24,25] Thus, alloys that are susceptible to accelerated attack should fail more quickly in this test than in an engine. On the other hand, alloys that perform well in this test for a fixed test time should perform well for even longer times in this application. How much the water vapor content could be further increased to accelerate laboratory testing is not known. Increasing the water content to, for example, 50% might result in a different type of attack mechanism that would not occur in an exhaust gas stream. If scale evaporation is an important mechanism, increasing the gas flow rate also could accelerate the testing.[12] However, the gas flow rate in a microturbine is such that exceeding that rate in a laboratory environment may not be feasible.

There is still a considerable amount of work to be done in order to develop a low-cost alternative to type 347 stainless steel. More confidence is required in the experimental results and longer-term data are needed before compositions will be scaled up to mill-sized heats and mill runs of foil made so that field testing can be conducted.

SUMMARY

In collaboration with industrial partners, the U.S. Department of Energy has a goal of developing advanced high-temperature microturbines that will achieve operating efficiencies approaching 40%. Type 347 stainless steel, currently used in microturbine recuperators, is not likely to meet the temperature and lifetime goals set by this program because of corrosion problems caused by water vapor in the exhaust gas. More highly alloyed stainless steels or Ni-base alloys are more corrosion-resistant in these environments but their cost may be prohibitive for this application. Laboratory results with model alloys suggest that increasing both the Ni and Cr contents to approximately 20% will improve the corrosion resistance in these environments. None of the minor alloy additions evaluated in this study had a significant effect on corrosion resistance except for Si which is already present in most commercial stainless steels. Long term laboratory and engine testing is needed to confirm the performance of these alloys.

ACKNOWLEDGMENTS

The authors wish to thank G. Garner at ORNL for performing the oxidation exposures, H. Longmire at ORNL for performing the metallography and L. Walker for performing the microprobe work. D. P. Stinton and I. G. Wright at ORNL reviewed the manuscript. The research was sponsored by the U.S. Department of Energy, Office of Power Technology, Distributed Energy Resources Program under contract DE-AC05-00OR22725 with UT-Battelle, LLC.

REFERENCES

1. J. H. Watts, Global Gas Turbine News, **39**(1), (1999): pp.4-8.
2. S. L. Hamilton, Modern Power Systems, **19**(9), (1999): pp.21-22.
3. Advanced Microturbine Systems Program, Plan for Fiscal Years 2000 Through 2006, U. S. Department of Energy, Office of Energy Efficiency and Renewable Energy, Office of Power Technologies, Washington, D. C. (March 2000)

4. M. E. Ward, Turbomachinery Technology Seminar Paper TTS006/395, 1995, Solar Turbines, Inc., San Diego, CA.
5. P. J. Maziasz and R. W. Swindeman, J. Eng. Gas Turbines and Power 124, (2002): p.1.
6. D. Caplan and M. Cohen, Corrosion 15, (1959): pp.57-62.
7. C. T. Fujii and R. A. Meussner, J. Electrochem. Soc. 110, (1963): p.1195; 111, (1964): p.1215.
8. G. C. Wood, I. G. Wright, T. Hodgkiess, D. P. Whittle, Werk. Korr. 21, (1970) p.900-10.
9. I Kvernes, M. Oliveira and P. Kofstad, Corrosion Science 17, (1977): p.237.
10. H. Nickel, Y. Wouters, M. Thiele and W. J. Quadakkers, Fresenius Journal Analytical Chemistry 361, (1998): pp.540-4.
11. B. A. Pint and J. M. Rakowski, NACE Paper 00-259, Houston, TX, presented at NACE Corrosion 2000, Orlando, FL, March 2000.
12. H. Asteman, J.-E. Svensson, M. Norell and L.-G. Johansson, Oxid. Metals 54, (2000): p.11-26.
13. V. Lepingle, G. Louis, D. Petelot, B. Lefebvre and J. C. Vaillant, Mater. Sci. Forum 369-372, (2001): p.239-46.
14. S. Henry, A. Galerie and L. Antoni, Mater. Sci. Forum 369-372, (2001): p.353-60.
15. B. A. Pint, R. W. Swindeman, K. L. More and P. F. Tortorelli, ASME Paper 2001-GT-445, presented at the International Gas Turbine & Aeroengine Congress & Exhibition, New Orleans, LA, June 4-7, 2001.
16. R. Peraldi and B. A. Pint, submitted to Mater. High Temp.
17. P. J. Maziasz, R. W. Swindeman, J. P. Montague, M. Fitzpatrick, P. F. Browning, J. F. Grubb and R. C. Klug, Materials at High Temperature 16, (1999): p.207-12.
18. B. A. Pint, K. L. More and P. F. Tortorelli, ASME Paper 2002-GT-30543, presented at the International Gas Turbine & Aeroengine Congress & Exhibition, Amsterdam, June 3-6, 2002.
19. Zs. Tökei, K. Hennesen, H. Viefhaus and H. J. Grabke, Materials Science Technology 16, (2000): p.1129-1138.
20. N. Otsuka, Y. Shida and H. Fujikawa, Oxidation of Metals 32, (1989): p.13-45.
21. W. J. Quadakkers, T. Malkow, J. Piron-Abellan, U. Flesch, V. Shemet and L. Singheiser, Proc. 4th Eur. Solid Oxide Fuel Cell Forum, Vol. 2, A. J. McEvoy ed. (Elsevier, Amsterdam, 2000) p.827-36.
22. K. Tamura, T. Sato, Y. Fukuda, K. Mitsuhata, H. Yamanouchi, Heat Resistant Materials II, K. Natesan, P. Ganesan and G. Lai eds., ASM International, Materials Park, OH, 1995, p.33-9.
23. D. T. Hoelzer, B. A. Pint and I. G. Wright, J. Nuclear Materials 283-287, (2000): p.1306-10.
24. J. Shen, L. Zhou and T. Li, Oxidation of Metals 48, (1997): p.347-56.
25. J. M. Rakowski, ASME Paper 2001-GT-360, presented at the International Gas Turbine & Aeroengine Congress & Exhibition, New Orleans, LA, June 4-7, 2001.

TABLE 1
ALLOY CHEMICAL COMPOSITIONS (WEIGHT %) AND AVERAGE GRAIN SIZES (µm)

Material	Cr	Ni	Mn	Mo	Si	C	N	Nb	Ti	Other	average grain size
Type 321	17	11	1						0.3		
Type 347	17	11	1.6	0.1	0.6	0.04	0.02	0.6	0.04		40µm
20/25/Nb	20	25	1.0	1.6	0.4	0.10	0.14	0.3	0.03	0.03Al	
Alloy 625	21	bal.		9				4		4 Fe	10
Alloy 214	16.0	bal.	0.2	0.01	0.08	0.05	<		0.01	3.5Fe,4.3Al	
Fe-16Cr-10Ni	15.8	9.9	<	<	<	<	<	<	<		n.d.
Fe-16Cr-30Ni	15.7	29.6	<	<	<	<	<	<	<		19µm
Fe-20Cr-10Ni	19.9	9.9	<	<	<	<	<	<	<		n.d.
Fe-20Cr-20Ni	19.7	20.1	<	<	0.01	<	<	<	<		14
Fe-20Cr-30Ni	19.6	30.1	<	<	0.01	<	<	<	<		13
Fe-20Cr-20Ni+	20.9	20.8	3.8	0.3	0.24	0.08	0.02	0.3	<		n.d.
Fe-10Cr	9.4	<	<	<	0.02	<	<	<	<		81
Fe-16Cr	15.7	<	<	<	<	<	<	<	<		97
Fe-20Cr	19.6	<	<	<	<	<	<	<	<		84
Fe-16Cr+Si	16.1	<	<	<	0.17	<	<	<	<		100
Fe-16Cr+La	15.9	<	<	<	<	<	<	<	<	0.3La	91
Fe-16Cr-1Mn	16.0	0.01	1.1	<	0.01	<	<	<	<		88
Fe-16Cr-2Mo	16.1	0.01	<	2.0	<	<	<	<	<		65

< indicates below the detectability limit of <0.01%

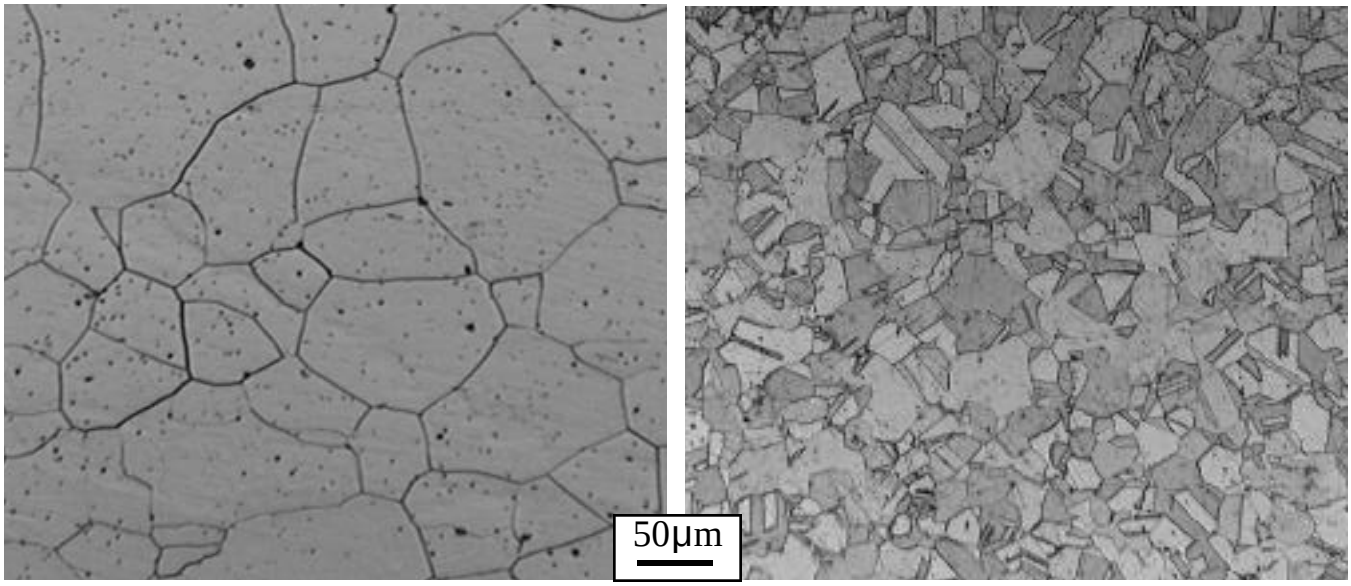

FIGURE 1. Light microscopy of rolled model alloys (a) Fe-20Cr and (b) Fe-20Cr-20Ni

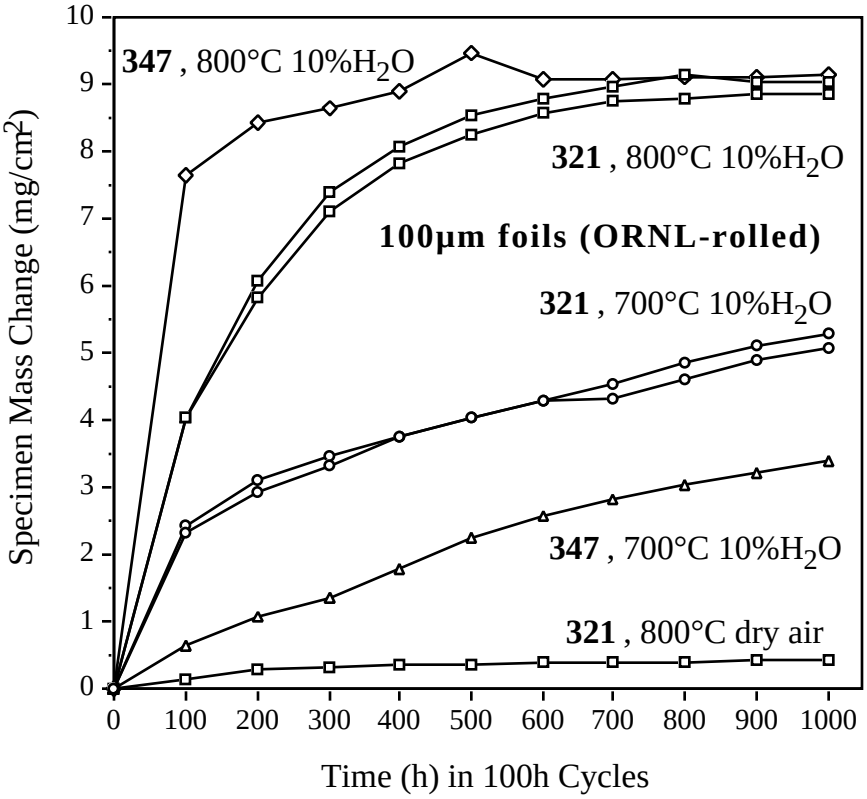

FIGURE 2. Mass change of stainless steel foils during 100h cycles at 700° and 800° in dry air or air plus 10% water vapor.

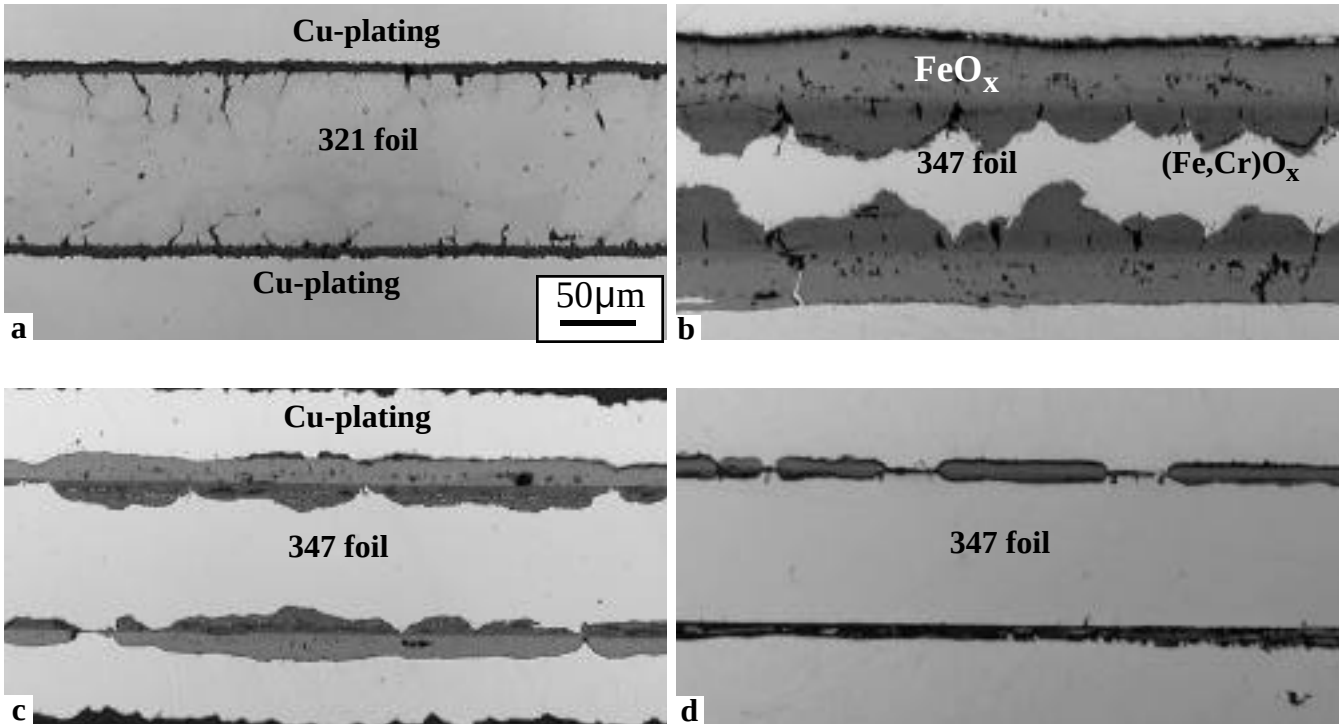

FIGURE 3. Light microscopy of polished cross-sections of ORNL-rolled 100µm foils (a) type 321 after 5000h (10, 500h cycles) at 800°C in dry air; and type 347 after 1000h (10, 100h cycles) in humid air at (b) 800°C, (c) 700°C and (d) 650°C.

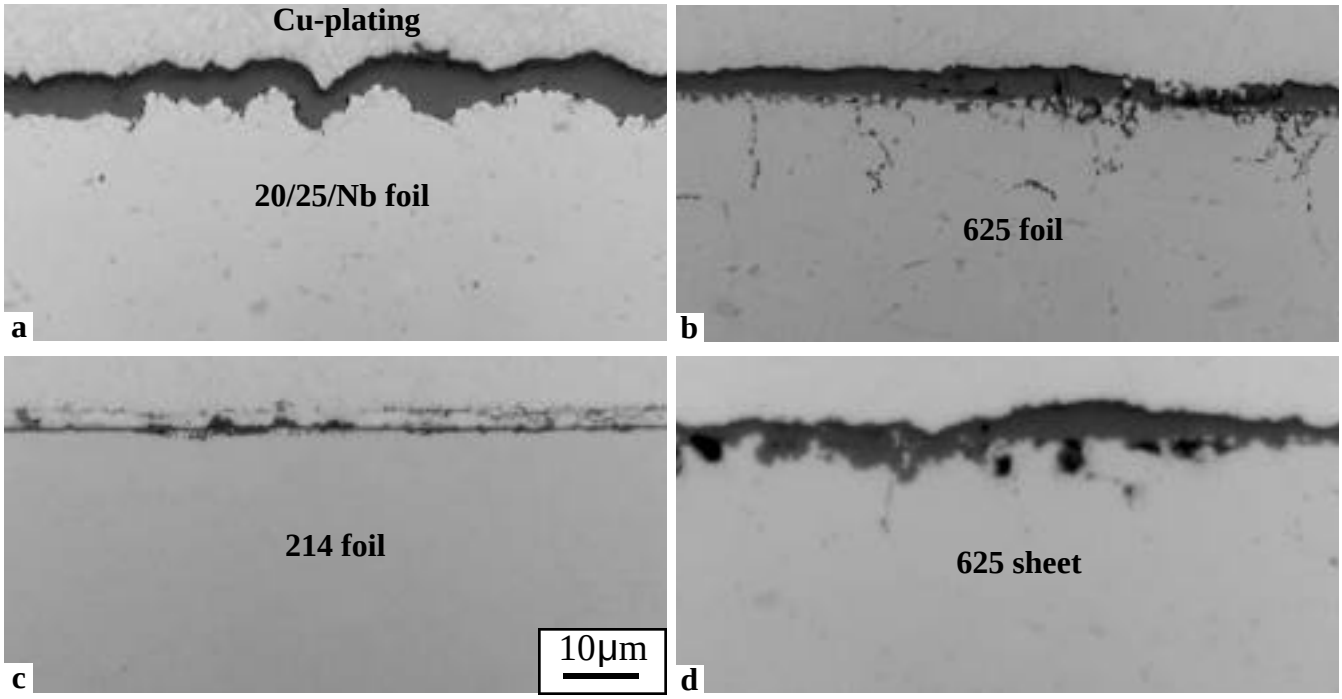

FIGURE 4. Light microscopy of polished cross-sections of ORNL-rolled foils exposed for 100h cycles at 800°C in air plus 10% H_2O: (a) 20/25/Nb for 6,000h, (b) alloy 625 for 6,000h and (c) alloy 214 for 5,000h; (d) shows the scale formed on 1mm thick alloy 625 sheet after 6,000h at 800°C in air plus 10% H_2O.

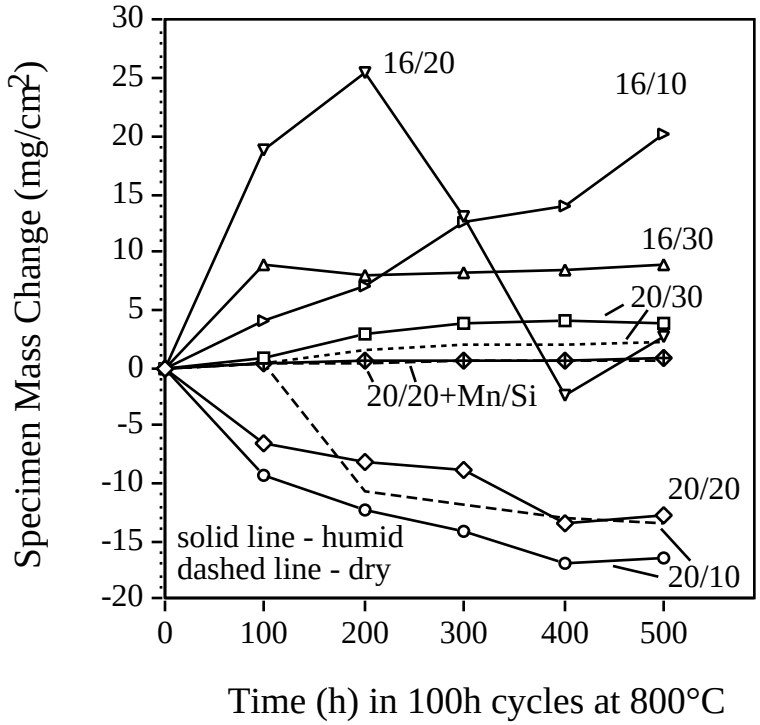

FIGURE 5. Specimen mass changes for model Fe-Cr-Ni alloys (specified by their Cr/Ni contents) during 100h cycles at 800°C in dry air (dashed line) and air plus 10%H_2O (solid line).

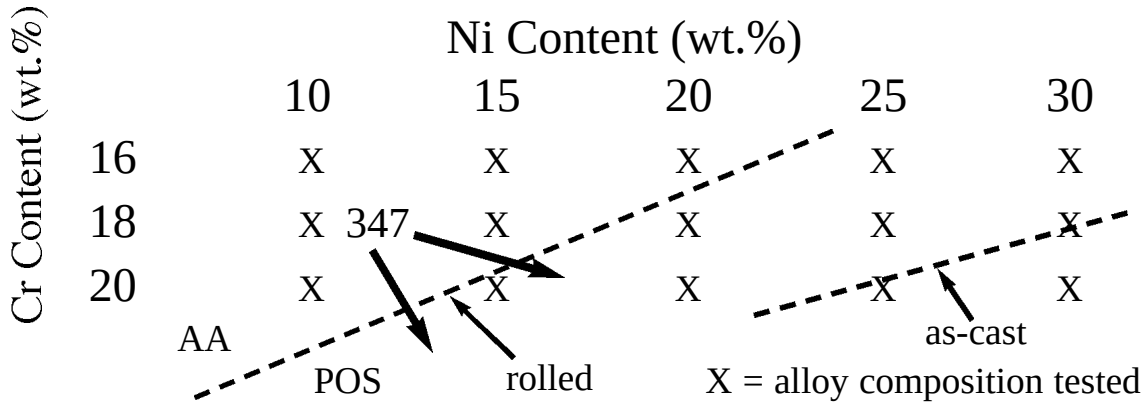

FIGURE 6. Schematic of the performance of the model Fe-Cr-Ni alloys at 700°C in 10% H_2O showing the composition line between the formation of a protective scale (POS) and accelerated attack (AA).

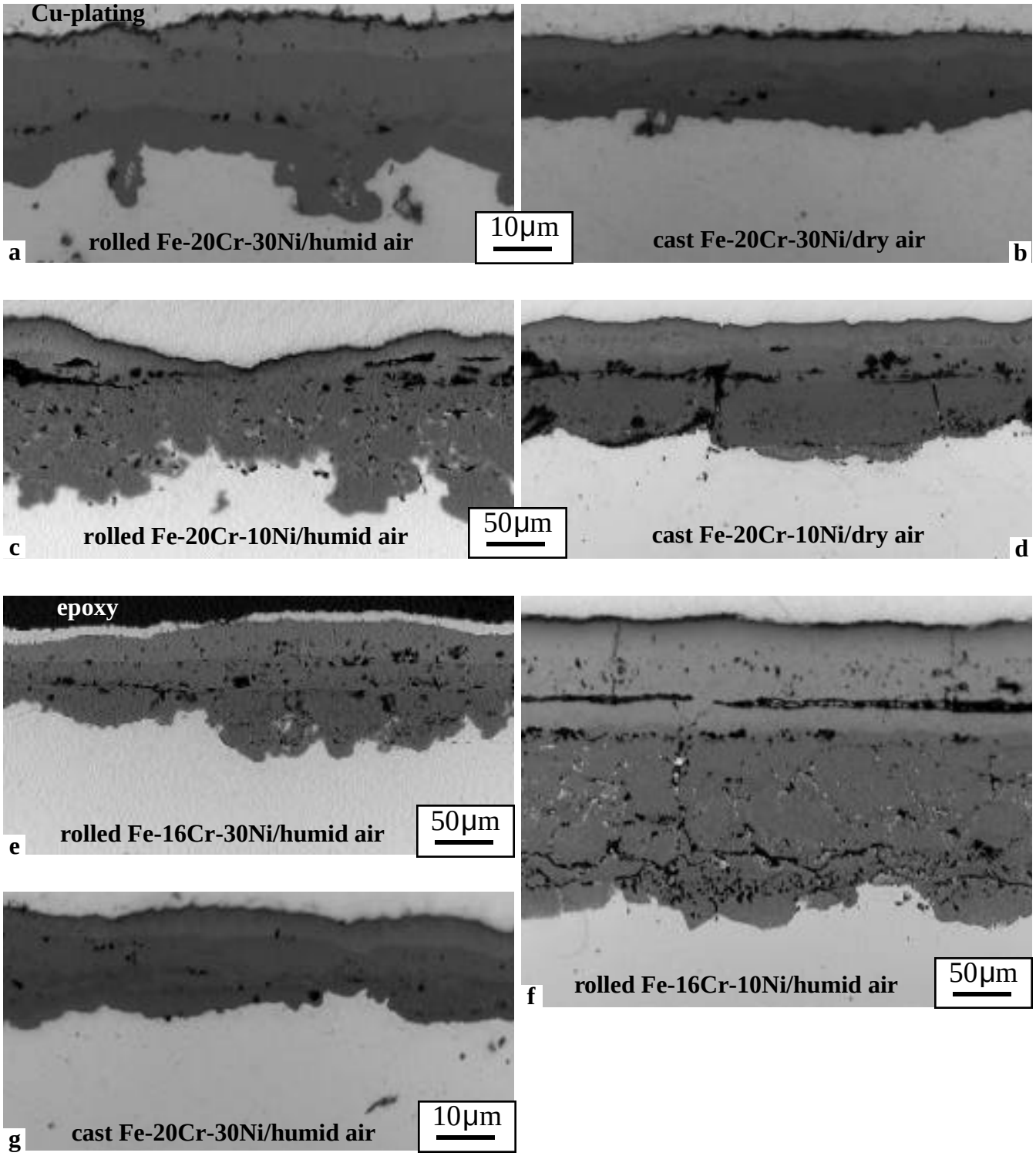

FIGURE 7. Light microscopy of polished cross-sections after 5, 100h cycles at 800°C for (a) rolled Fe-20Cr-30Ni in humid (10% water vapor) air, (b) as-cast Fe-20Cr-30Ni in dry air, (c) rolled Fe-20Cr-10Ni in humid air, (d) as-cast Fe-20Cr-10Ni in dry air, (e) rolled Fe-16Cr-30Ni in humid air, (f) rolled Fe-16Cr-10Ni in humid air and (g) as-cast Fe-20Cr-30Ni in humid air.

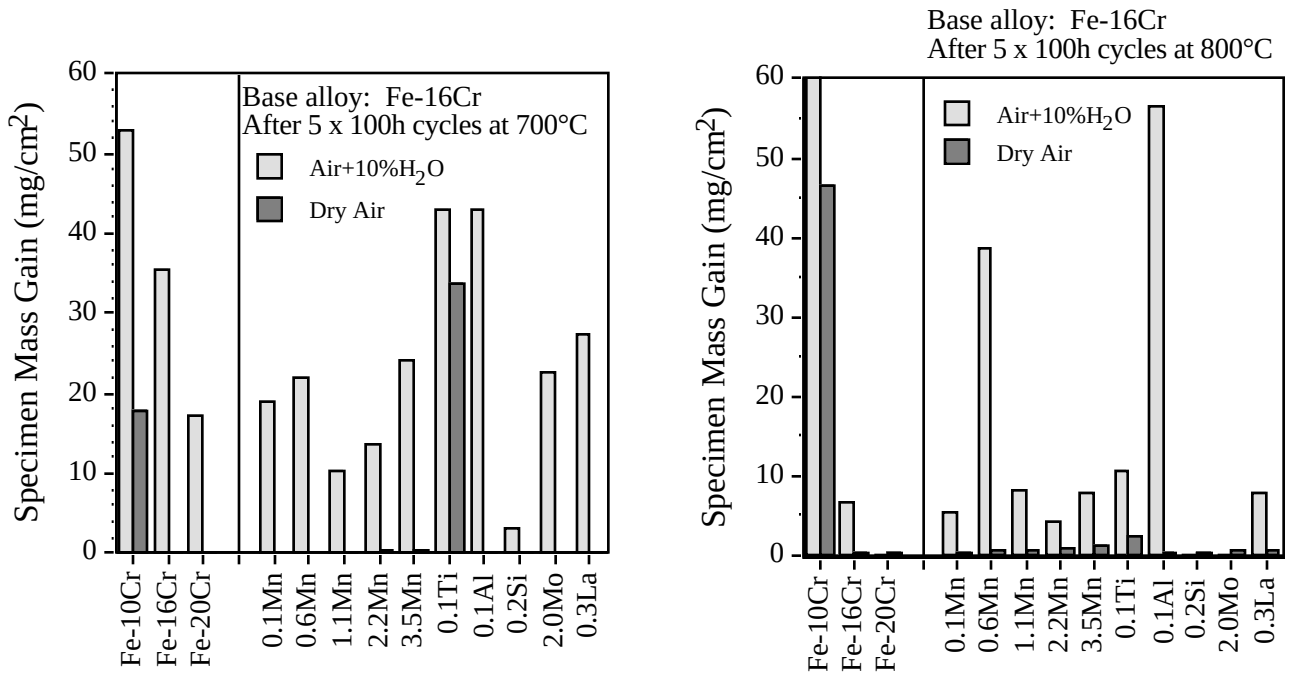

FIGURE 8. Specimen mass gains for ferritic model alloys after 5, 100h cycles in dry and humid air at (a) 700°C and (b) 800°C. The minor alloy additions were made to a base alloy of Fe-16Cr.

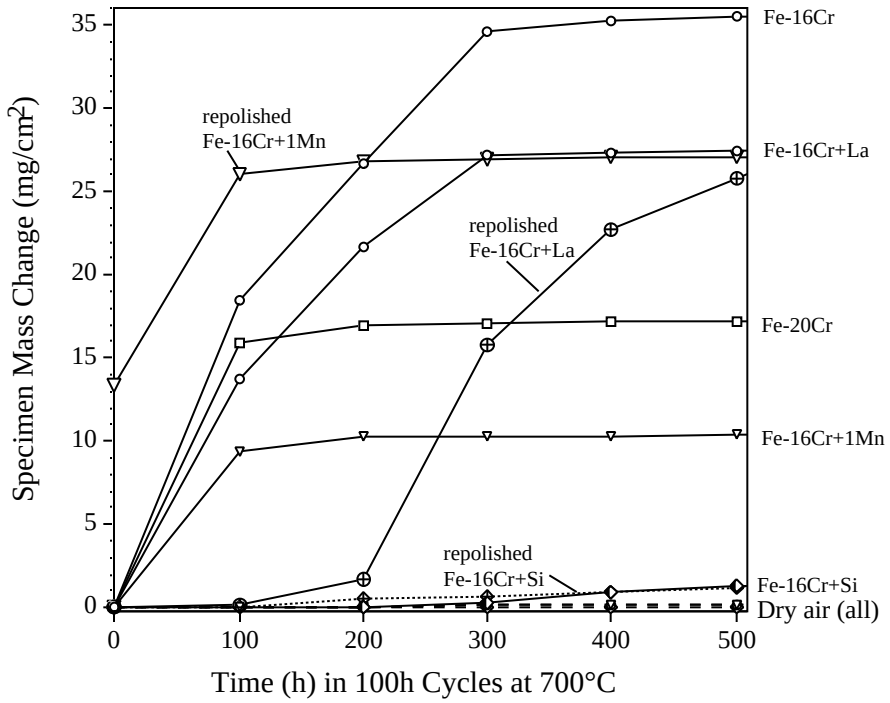

FIGURE 9. Specimen mass changes for model Fe-Cr alloys during 100h cycles at 700°C in air plus 10%H_2O. Three specimens were repolished (i.e. the scale was removed) after 100h but similar behavior was observed compared to the specimens that were not repolished.